Int. J. Heat Mass Transfer. Vol. 28, No. 2, pp. 319–330, 1985
Printed in Great Britain

0017–9310/85 $3.00 + 0.00

The transfer of heat by natural convection between bodies and their enclosures

R. O. WARRINGTON, JR.
Mechanical Engineering Department, Montana State University, Bozeman, MT 59717, U.S.A.

and

R. E. POWE
Office of Research, Mississippi State University, Mississippi State, MS 39726, U.S.A.

(*Received* 22 *July* 1982 *and in revised form* 16 *April* 1984)

Abstract—Natural convection heat transfer between concentrically located isothermal spherical, cylindrical and cubical inner bodies and their isothermal cubical enclosure was experimentally investigated. Comparisons were made with the existing data for these same inner bodies and a spherical enclosure. In addition, temperature distributions and flow visualization data were obtained for most of those geometries. Comparisons made between the spherical and cubical enclosure, for the same inner body types, showed that the cubical enclosure resulted in a larger Nusselt number for a given Rayleigh number and inner body size. Heat transfer data taken with a non-isothermal inner body showed that the isothermality conditions on the inner body could be relaxed. All of the heat transfer data was correlated with an average deviation of less than 14%. Overall, the effect of the enclosure shape was small so long as the appropriate length scale is employed.

INTRODUCTION

THE AMOUNT of work accomplished in the area of natural convection heat transfer within enclosures has increased over tenfold in the last 20 years. Despite the intensity of the effort, knowledge in this area is still limited. The demands for additional information in this area have also increased, as evidenced by the growing number of applications for natural convection heat transfer within enclosures. General areas of application include: nuclear design, electronic packaging, residential heating, and more recently in the solar energy field, solar collector design and utilization of natural circulation for energy storage systems and passive solar heating.

The majority of the work accomplished in the area of natural convection heat transfer within enclosures has been experimental. The coupling and non-linearity of the governing equations, the fact that the boundary layer approximations are not valid for enclosures and the complicated geometries involved have forced experimental solutions. The relatively few analytical and numerical solutions available are generally limited in applicability.

Early experimental studies in enclosures include the work by Batchelor [1], Poots [2], Eckert and Carlson [3], and Elder [4]. These and other early studies began to explain the basic heat transfer and fluid flow phenomena in enclosures and paved the way for much of the experimental work that followed. Experimental investigations of natural convection between a body and its enclosure have been limited to primarily cylindrical and spherical inner and outer geometries. Many researchers [5–12] have studied natural convection heat transfer and fluid flow in cylindrical annuli. These studies have been both experimental and numerical and have considered both oscillatory and non-oscillatory flows. Bishop and others [13–18] experimentally studied natural convection from concentric spheres and cylinders and eccentric spheres to a spherical enclosure. Their work included flow visualization studies. Powe [19] has studied the bounding effects for both the spherical and cylindrical inner bodies. Few numerical solutions exist for these geometries and those that do, such as the solution by Mack and Hardee [20], are limited in applicability.

More recently Powe *et al.* [21, 22] experimentally studied natural convection from a cubical inner body to a spherical enclosure. These two works also summarize all of the spherical enclosure flow and heat transfer studies. Warrington and Crupper [23] investigated natural convection from cylindrical tube bundles in the horizontal and vertical position to a cubical enclosure.

Other areas that have received some attention are approximate solutions and methods for correlating the heat transfer data [24–27]. In particular the generalized integral method of Raithby and Hollands [26, 27] has been applied to several of the geometries mentioned above with good success.

The primary intent of this investigation is to experimentally determine the heat transfer and temperature distributions between isothermal spherical, cylindrical and cubical inner bodies and their isothermal cubical enclosure. These data will be compared with past investigations [13–18, 21, 22] which utilized basically the same inner bodies and fluids but with a spherical enclosure. The effect of the enclosure on the overall heat transfer and the

NOMENCLATURE

a	any characteristic length
A_i	inner body surface area
b	distance traveled by the boundary layer on the inner body
c_1, c_2	empirically determined constants
c_p	specific heat at constant pressure
g	acceleration of gravity, 9.81 m s^{-2}
Gr_a	Grashof number, $\rho^2 g\beta (T_i - T_o)a^3/\mu^2$
$\bar{h}$	average heat transfer coefficient, $q_{conv}/A_i\Delta T$
G	(total outer body height minus the total inner body height)/2
k	thermal conductivity
k_{eff}	effective thermal conductivity
L	gap width or hypothetical gap width, $R_o - R_i$
Nu_a	Nusselt number, $\bar{h}a/k$
Pr	Prandtl number, $c_p\mu/k$
Q	ratio of q_{conv}/q_{cond}
q_{cond}	heat transfer by conduction
q_{conv}	heat transfer by convection
Ra_a	Rayleigh number, $\rho^2 g\beta(T_i - T_o)a^3 c_p/\mu k$
Ra_a^*	modified Rayleigh number, $Ra_a(L/R_i)$
r	local position of thermocouple probe ($r = 0$ at center of test space)
r_i	inner body radius, except for cubes where it is half the side length
r_o	outer body radius (spherical outer body)
$r(\theta)$	distance from the center of the inner body to the surface of the inner body
R_i	inner body radius for the spheres, but for the cylinders and cubes it is a hypothetical radius of an inner sphere of a volume equal to the cylindrical or cubical inner body
R_o	outer body hypothetical radius equal to the radius of a sphere having a volume equal to the volume of the outer body
T	local temperature
T_{am}	arithmetic mean temperature, $(T_i + T_o)/2$
T_i	inner body temperature
T_o	outer body temperature
ΔT	temperature difference, $T_i - T_o$.

Greek symbols

β	thermal expansion coefficient
θ	temperature probe angular location
μ	dynamic viscosity
ρ	density.

temperature field was determined. Correlation equations to predict the heat transfer between these somewhat arbitrarily shaped inner and outer bodies was determined. Temperature field and visualization data are presented which will aid in the understanding of the heat transfer and fluid flow phenomena.

APPARATUS AND PROCEDURE

The heat transfer apparatus is shown in Fig. 1 with a spherical inner body in the test space. The cubical outer body was constructed of 1.27 cm thick, type 6061 aluminum, with an inner 26.67 cm cubical chamber. This outer body was cooled and kept isothermal to within 2 K by six separately controlled rectangular water jackets (3.175 cm wide). A closed system consisting of a chiller, pump, and storage reservoir was used to cool the outer body. Flow visualization data were obtained with a similar apparatus made of clear polyvinyl and painted black except for a light source slot placed vertically on one side and one clear side which allowed photographs to be taken of the flow patterns. Thermal boundary conditions were the same for flow visualization studies and heat transfer studies.

The inner body geometries and test fluids used with the spherical enclosure (used in this study for comparison) and the cubical enclosure (new data) are listed in Table 1. Basically the same inner body geometries and fluids were used in the present investigation. The rotated cube data represents a rotation of 45° horizontally from the parallel face position.

The inner bodies were supported in the test space by a stainless steel stem 1.27 cm in diameter. This support

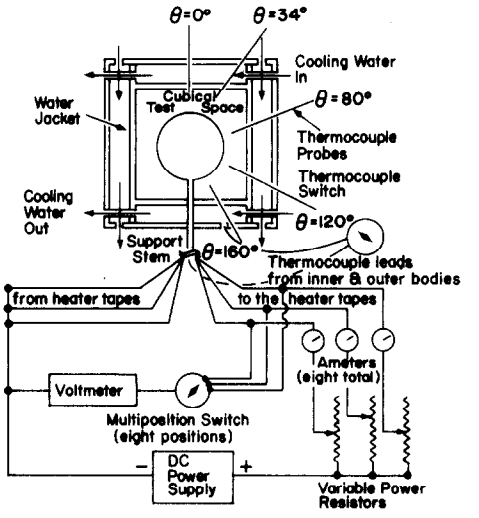

FIG. 1. Heat transfer apparatus.

Table 1. Geometries and test fluids used with spherical and cubical enclosures

Inner body (cm)	Air	Water	20 CS	350 CS	Glycerin	r_i/r_o	L/r_i	L/R_i	b (cm)
Spherical inner bodies (Bishop *et al.* [13], Scanlan *et al.* [14], spherical enclosure)									
Diameter									
10.16	×					0.40	1.50	1.50	15.95
12.70	×					0.50	1.00	1.00	19.94
15.24	×					0.60	0.67	0.67	23.93
20.23	×					0.80	0.25	0.25	31.93
8.89		×				0.36	1.18	1.81	13.97
11.43		×	×	×		0.46	1.18	1.18	17.96
13.97		×	×	×		0.56	0.79	0.79	21.95
17.78		×	×	×		0.71	0.40	0.40	27.94
22.86		×	×	×		0.92	0.09	0.09	35.92
Cylindrical inner bodies (Weber *et al.* [15], McCoy *et al.* [17], spherical enclosure)									
Diameter × length									
11.43 × 17.15		×				0.46	0.98	0.81	23.67
11.43 × 22.23			×			0.46	0.84	0.63	28.75
13.97 × 18.11		×	×	×		0.56	0.66	0.58	26.10
13.97 × 22.38		×	×	×		0.56	0.55	0.44	30.35
17.78 × 20.32		×				0.71	0.34	0.32	30.48
17.78 × 22.53		×				0.71	0.28	0.25	32.69
22.86 × 23.70		×				0.92	0.07	0.97	36.73
Cubical inner bodies (Powe *et al.* [22], spherical enclosure)									
Side length									
6.39	×	×	×	×	×	0.26	2.67	2.15	12.78
10.64	×	×	×	×	×	0.43	1.10	0.89	21.29
12.56		×	×	×	×	0.50	0.75	0.60	25.12
Spherical inner bodies (new data, cubical enclosure)									
Diameter									
11.43	×	×	×		×	0.43	1.89	1.89	17.96
17.78	×	×	×		×	0.67	0.86	0.86	27.94
22.86	×	×	×		×	0.86	0.45	0.45	35.92
Cylindrical inner bodies (new data, cubical enclosure)									
Diameter × length									
11.43 × 16.13	×	×	×		×	0.43	1.72	1.47	22.66
11.43 × 22.61	×	×	×		×	0.43	1.54	1.14	29.14
17.78 × 20.57	×	×	×		×	0.67	0.79	0.73	30.73
17.78 × 22.61	×	×	×		×	0.67	0.74	0.66	32.77
Cubical inner bodies (new data, cubical enclosure)									
Side length									
10.16	×	×	×		×	0.38	2.02	1.62	20.32
12.70	×	×	×		×	0.48	1.36	1.10	25.40
16.26	×	×	×		×	0.61	0.79	0.64	32.52
16.26 (rotated)	×	×	×		×	0.61	0.79	0.64	32.52

stem housed the inner body thermocouples and power leads and was insulated on its outside surface to minimize heat transfer to the test space. Access to the inner bodies was obtained through a 25.4 cm diameter removable circular plate on the top inner face of the outer body and a completely removable outer face, also on the outer body. All the test liquids were gravity fed into the test space through the bottom of the cubical enclosure.

Each inner body was constructed using a number of heater tapes which could be independently controlled. Thus, a monotonic temperature variation could be attained from top to bottom along the inner body. Likewise, the inner bodies could be kept isothermal by adjusting the power to the heater tapes. The number of tapes per inner body varied with both the size and type of inner body, varying from four to a maximum of eight. The spherical and cylindrical inner bodies were fabricated from 0.064 cm thick copper and the cubes from 0.318 cm thick copper, which contributed to the isothermality of the inner bodies. The temperature variation (defined as the local maximum T minus local minimum T divided by $T_i - T_o$) was less than 10% for all of the data except for a few of the water data points at the highest temperature differences. All inner and outer body temperatures were measured using thermocouples imbedded in the bodies.

In addition to the isothermal inner body data, over 100 data points were taken with a large temperature variation imposed on the inner bodies. Temperatures were adjusted on the inner bodies to give maximum temperature variations from top to bottom and bottom to top. The average temperature variation for these data was 58.50%.

Temperature profiles were obtained in the test space by traversing a thermocouple probe through nine

thermocouple probe ports located in the outer body. These ports consisted of one common and four additional ports on each of two separate axes. One axis was on a vertical plane through the center of the cube while the other was the vertical plane through the edge of the cube. The five ports in each axis were at 0°, 34°, 80°, 120° and 160° measured downward from the top vertical axis. One of these planes is shown in Fig. 1. A vernier caliper attached to the thermocouple probe fixed the location of the probe within the test space to within 0.0025 cm. The thermocouples used to measure the temperature profiles had head diameters less than 0.05 cm and they were not shielded. The air temperature profiles were generally unsteady and qualitative in nature.

The 44 geometry/fluid combinations listed in Table 1 were used to obtain over 800 heat transfer data points with the cubical enclosure. In addition, temperature profiles were obtained for selected heat transfer runs. Flow visualization studies were also made for air, 20 CS silicone oil, and glycerin in the test space. Flow patterns were obtained for air and the liquids (20 CS silicone oil and glycerin) by using smoke and fluorescent paint particles, respectively, for the tracer particles.

With one of the fluids in the test space, power was applied to the inner body and after equilibrium was established (approximately 2 h), the inner and outer body temperatures and the total power input to the inner body were recorded. The heat transferred by natural convection was obtained by subtracting from the total power input the 1-D conduction losses down the insulated support stem and, in the case of air, the radiation from the inner body to the outer body (the liquids are opaque to radiation). The radiation losses were determined by evacuating the test space ($<20\ \mu$m Hg) and taking the difference between the total power input and the conduction losses down the stem. The conductive heat transfer losses were less than 4 and 1% of the free convection heat transfer for air and the liquids, respectively. Flow visualization studies revealed no flow disturbance near the stem, and this implies that there was little heat transfer from the insulated stem to the test fluids. The radiative losses for air were of the order of 70% of the total heat transferred from the inner bodies.

HEAT TRANSFER RESULTS

Equations of the form

$$Nu_L = c_1 Ra_L^{c_2} \tag{1}$$

$$Nu_L = c_1 Ra_L^{*c_2}, \quad \text{where } Ra_L^* = Ra_L\left(\frac{L}{R_i}\right) \tag{2}$$

$$Nu_L = c_1 Ra_L^{c_2}\left(\frac{L}{R_i}\right)^{c_3} Pr^{c_4} \tag{3}$$

$$Nu_b = c_1 Ra_b^{c_2} \tag{4}$$

$$Nu_b = c_1 Ra_b^{*c_2} \tag{5}$$

$$Q = \frac{q_{conv}}{q_{cond}} = \frac{k_{eff}}{k} = c_1 Ra_L^{c_2} \tag{6}$$

and

$$Q = c_1 Ra_L^{*c_2} \tag{7}$$

have been used with considerable success with the spherical enclosure data [13–17, 22]. These equations and others were also used to correlate the cubical enclosure heat transfer data.

All of the fluid properties were evaluated at the arithmetic mean of the inner and outer body temperatures. The hypothetical gap width and boundary layer length which have been used in the investigations referenced above were also used as the characteristic dimension in this study. The hypothetical gap width, $L = (R_o - R_i)$, is defined as the distance from an imaginary outer sphere whose volume is equal to the volume of a cube to an imaginary (in the case of the cylindrical and cubical inner bodies) inner sphere whose volume is equal to the volume of the inner body. The boundary layer length, first proposed by Lienhard [25] for infinite atmosphere natural convection, is the distance traveled by the boundary layer on the inner body assuming no flow separation. For the spheres, this distance was one-half the circumference of the sphere, for the cylinders it was the cylinder length plus one-half the circumference of the hemi-spherical end caps of the cylinders, and for the cubes this distance was twice the cube side length. This is a physically significant length parameter which has been used in data correlation in addition to length scales which are computationally convenient.

All of the heat transfer correlations presented below were obtained using a standard least-squares curve fitting technique. The deviation referred to below is the absolute difference between the data and the equation value divided by the data value and the average percent deviation is the sum of these individual deviations divided by the total number of data points. The overall experimental error was small and the data were sufficiently precise so that statistical methods to prove the following functional relationships were not necessary. In the discussions that follow referral to a particular inner and outer body combination, for example cylinder–cube, the inner body will always be given first.

Correlations for each inner body are given in terms of Nu_L and Ra_L in Figs. 2–4 for the spherical, cylindrical and cubical inner body types, respectively. In each of these figures, for a given Rayleigh number, the Nusselt number decreased with an increase in the size of the inner body. As has been explained by previous researchers [17, 23] this decrease in Nusselt number may be caused not only by a possible decrease in the heat transfer but also by an increase in the surface area of the inner body. Each of these figures exhibits a fairly significant geometric effect and very little Prandtl number effect. The geometric effect was reduced significantly, though not eliminated, by correlating the

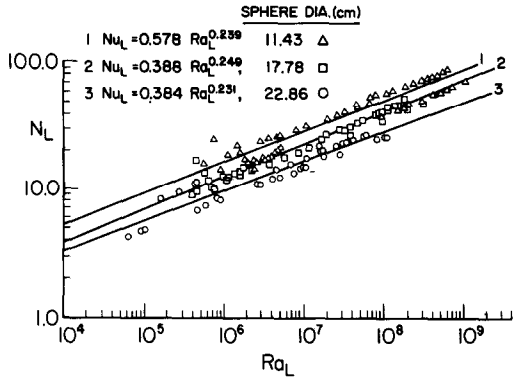

FIG. 2. Heat transfer correlations for all of the sphere–cube data and each individual inner body.

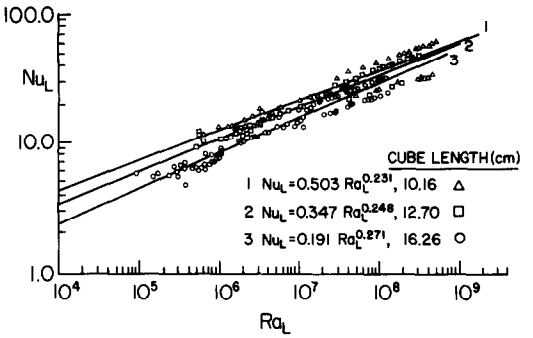

FIG. 4. Heat transfer correlations for all of the cube–cube data and each individual body.

data with the modified Rayleigh number and using the boundary layer length as the characteristic dimension.

The cube–cube geometry presented the possibility that a horizontal rotation of the inner body about its vertical axis might effect the heat transfer results. Figure 5 compares the 16.26 cm cube in its standard position (parallel faces between the inner and outer cubes) and a 45° rotation of the cube about its vertical axis. As can be seen in this figure, there is virtually no effect of the cube rotation on the heat transfer results.

Figure 6 is a direct comparison between the 26.67 cm cubical enclosure and the 24.96 cm diameter spherical enclosure. For the same size inner body the cubical enclosure data has a higher Nusselt number than the spherical outer body. This would be expected since the larger enclosure more closely approximates natural convection to an infinite atmosphere. In addition, the 3-D flows induced by the cubical enclosure (as evidenced in the flow visualization work) would also enhance the heat transfer. This difference in the Nusselt numbers decreased as the inner body size decreased indicating a smaller outer body effect. Each of the inner body types exhibited these trends.

All of the heat transfer results discussed thus far have been for isothermal inner and outer bodies. The effects of a non-isothermal inner body are now considered. Figure 7 shows the effects of a non-isothermal inner body temperature on the heat transfer results. Variation of the inner body temperature, defined previously, was 32.2% for the 16.26 cm cube and 20 CS fluid and 40.8% for the 10.16 cm cube and glycerin. The inner body temperature, T_i, was evaluated by computing the arithmetic mean of the local temperature distributed over the inner body. The solid symbols in Fig. 7 (non-isothermal data) are divided into a group of points above and below the corresponding open symbol. The points above the isothermal inner body data points represent an inner body with a maximum temperature at the top of the body and a minimum temperature at the bottom. The points below represent just the opposite temperature distribution on the inner body. A higher temperature in the upper region, a region of substantial convective activity, would tend to augment the driving potential for the heat transfer resulting in a larger Nusselt number. Similar results were obtained for the other geometries and fluids. The effects for the water data, which had an average temperature variation of 116%, were somewhat greater while the air data, with an average temperature variation of only 22.4%, exhibited a smaller effect than that shown in Fig. 7. When all of the non-isothermal heat transfer data (over 100 data

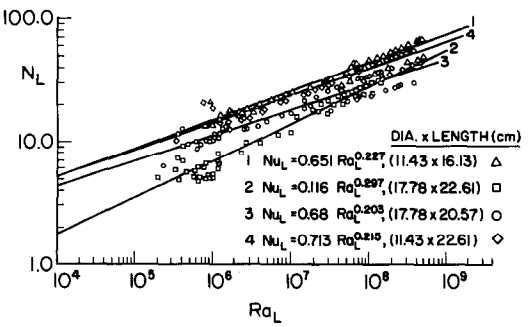

FIG. 3. Heat transfer correlations for all of the cylinder–cube data and each individual inner body.

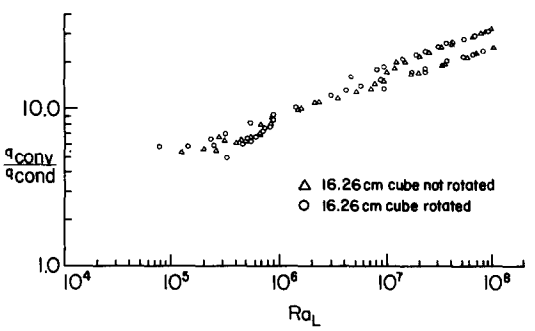

FIG. 5. Comparison of the heat transfer for rotated cube with the data for the cube in its standard position.

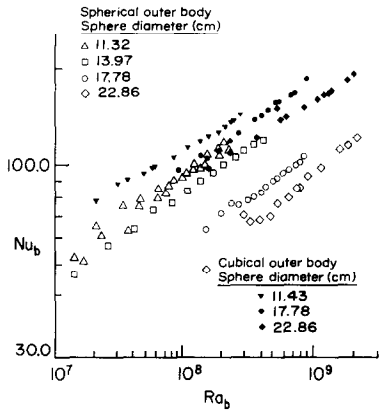

FIG. 6. Comparison of the spherical inner bodies with the cubical and spherical enclosures for the 20 CS fluid.

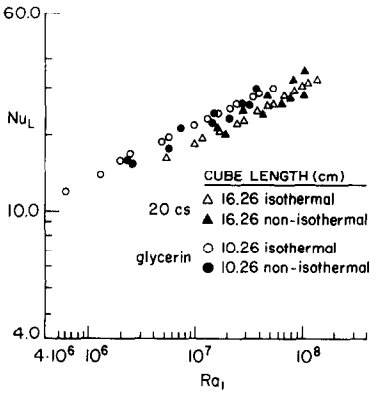

FIG. 7. Comparison of the isothermal inner body data with the non-isothermal inner body data for the 10.16 and 16.26 cm cubical inner bodies.

points) were compared with the isothermal data it was found that the non-isothermal data were well represented by the isothermal data heat transfer correlations. This was true even when the data for a maximum temperature at the top of the inner body was considered separately from the data for the maximum temperature at the bottom of the inner body. In fact, the increase in the average deviation for any of the correlations presented below never exceeded 3.1%. The relaxation of the isothermal boundary conditions on the inner body increase the applicability of all of the correlations presented in this study.

All of the heat transfer data for this study and for the previous spherical enclosure work is shown in Figs. 8–10. In making comparisons between these figures it should be noted that the vertical axis scale in Fig. 8 is only half the vertical axis scales in Figs. 9 and 10. For each figure, the solid symbols represent the cubical enclosure data and the open symbols represent the spherical enclosure data. All of the conduction solutions used in q_{cond} in Fig. 9 were obtained using standard finite differences. The curved surfaces of the inner bodies were approximated by using the closest grid point. The difference model was solved using successive over-relaxation.

Evident from Figs 8–10 is the effect of the outer body geometry on the overall heat transfer. This effect can also be shown by comparing the following heat transfer correlations for all of the enclosure data

$$Nu_b = 0.954 Ra_b^{0.208} \tag{8}$$

with an average deviation of 18.51% with

$$Nu_b = 0.585 Ra_b^{*0.236} \tag{9}$$

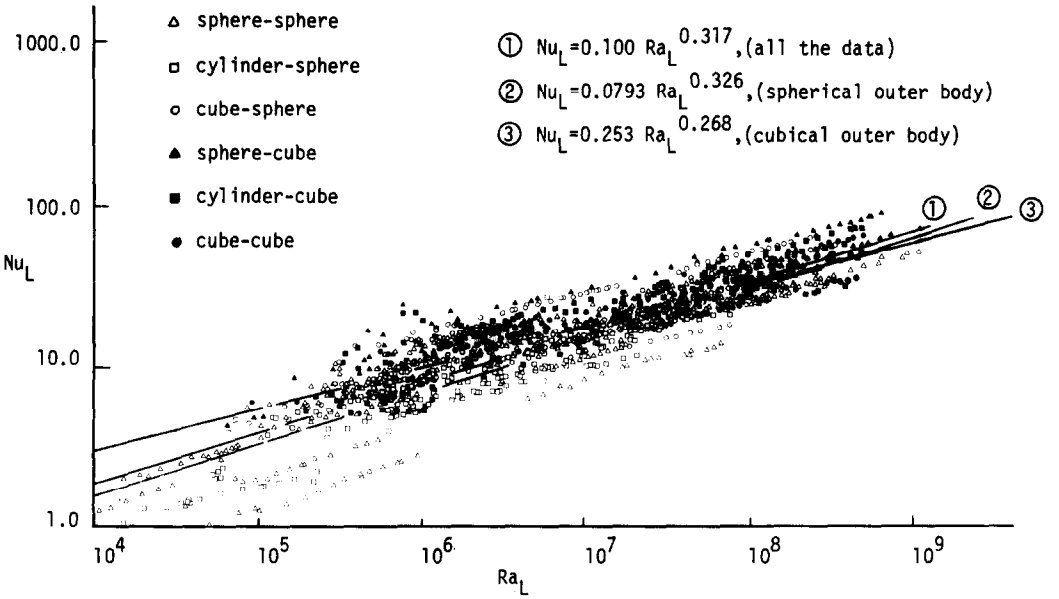

FIG. 8. Heat transfer correlations for all of the heat transfer data and each enclosure type.

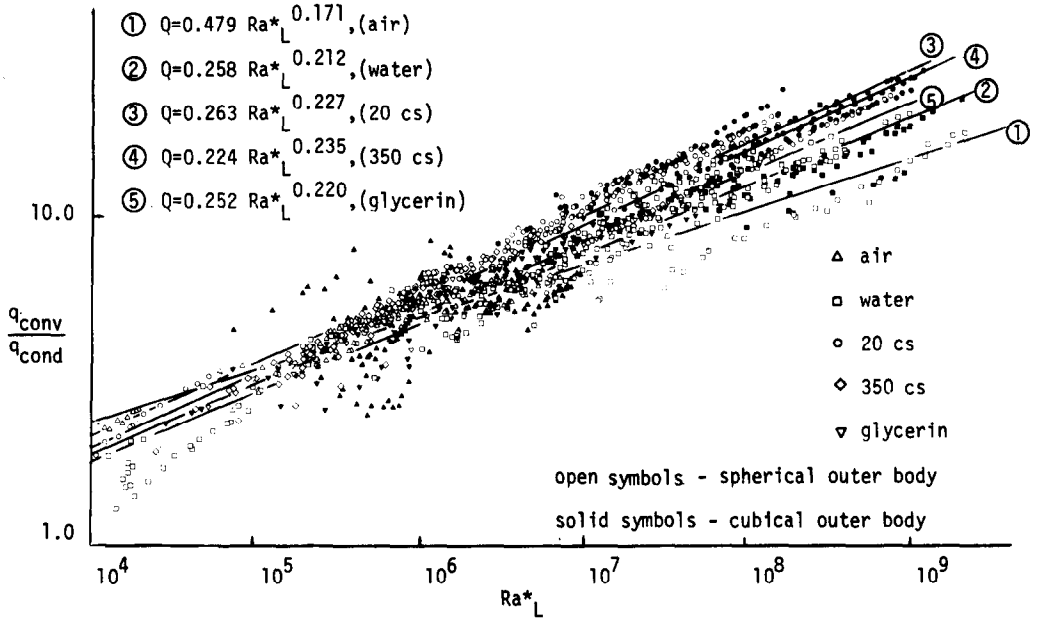

FIG. 9. Heat transfer correlations for all of the enclosure data and each individual fluid.

with an average deviation of 14.75%. Equation (8) is based solely on the inner boundary layer length and equation (9) includes the outer body effects in the modified Rayleigh number.

Solutions of natural convection heat transfer problems like the one we have been addressing can be divided in three regimes based on L/R [19]. These regimes are: (1) infinite atmosphere solution for large L/R_i, (2) enclosure solutions for moderate L/R_i and (3) conduction solutions for small L/R_i. It would be expected then that as L/R_i decreased q_{conv}/q_{cond} would become the superior dependent correlating parameter. To verify this statement, the heat transfer data was correlated using only geometries with $L/R_i \leqslant 0.66$ and $L/R_i \leqslant 0.45$. The results showed that the advantage of q_{conv}/q_{cond} over the Nusselt number increased since the average deviation decreased by several percent.

The best correlation for all the spherical and cubical

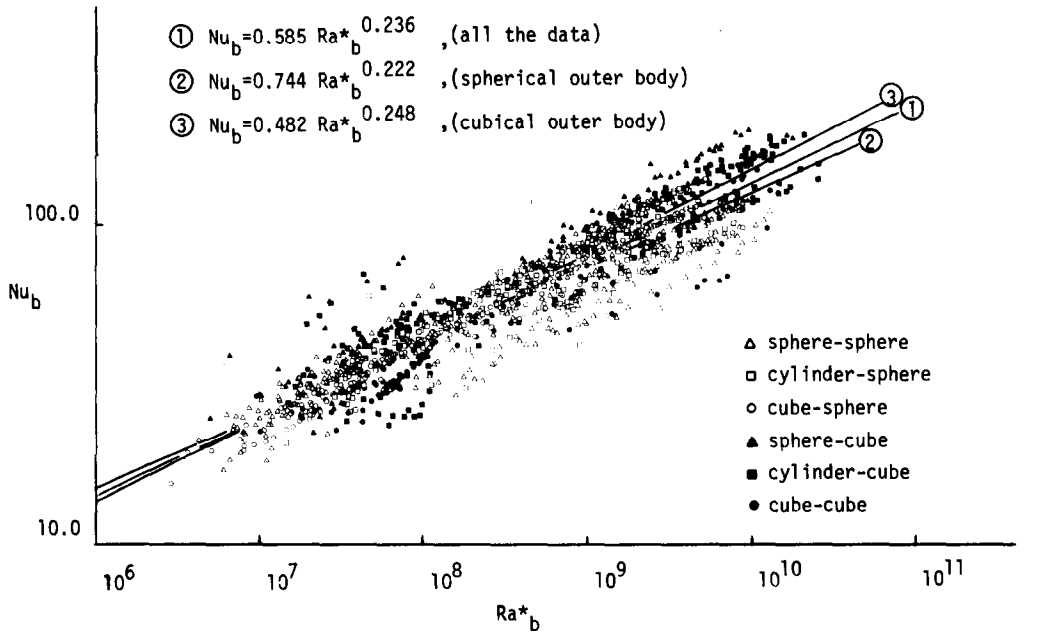

FIG. 10. Heat transfer correlations for all of the heat transfer data and each enclosure type.

Table 2. Correlations for the heat transfer data

Fluid	Equation number	Empirical constants C_1	C_2	C_3	C_4	Average percent deviation	Percent of data within ±20% of equation
		Correlation equations for the sphere–cube geometry					
All	2	0.369	0.253			13.52	77.37
	3	0.456	0.238	0.361	0.00665	12.36	83.94
	5	0.533	0.248			12.61	77.37
		Correlation equations for the cylinder–cube geometry					
All	2	0.288	0.261			19.24	70.77
	3	0.418	0.239	0.687	0.00403	14.27	76.41
	5	0.593	0.239			15.62	76.92
		Correlation equations for the cube–cube geometry					
All	2	0.267	0.260			12.09	86.39
	3	0.295	0.249	0.339	0.0217	10.17	91.62
	5	0.377	0.256			12.12	89.00
		Correlation equations for all the enclosure data					
All	1	0.100	0.317			30.22	42.71
	2	0.188	0.282			18.67	63.09
	3	0.396	0.234	0.496	0.0162	13.50	77.90
	5	0.585	0.236			14.75	77.12
	7	0.247	0.222			15.20	74.06
Air	2	0.173	0.299			14.31	77.18
	5	0.833	0.237			14.22	78.84
	7	0.479	0.171			13.54	81.74
Water	2	0.145	0.284			13.30	78.79
	5	0.720	0.220			14.30	74.70
	7	0.258	0.212			14.86	75.90
20 CS	2	0.106	0.319			8.46	91.67
	5	0.222	0.288			8.94	94.33
Glycerin	2	0.188	0.291			11.85	81.87
	5	0.485	0.248			9.10	91.76
	7	0.252	0.220			8.19	92.86

enclosure data is

$$Nu_L = 0.396 Ra_L^{0.234} \left(\frac{L}{R_i}\right)^{0.496} Pr^{0.0162} \quad (10)$$

with an average deviation of 13.50%.

For all of the enclosure data the best equation involving a single independent correlating parameter was

$$Nu_b = 0.585 Ra_b^{*0.236} \quad (11)$$

which had an average deviation of 14.75%. For $L/R_i < 0.45$ the following equation could be used

$$Q = 0.200 Ra_L^{*0.239}. \quad (12)$$

This equation has an average percent deviation of 13.76. Other correlations of the data are listed in Table 2. These data are valid for Prandtl numbers in the range 0.707–1.4×10^4, Rayleigh numbers based on gap width and boundary layer length in the range 1.8×10^3–1.1×10^9 and 4.6×10^5–4.0×10^{10}, respectively, and modified Rayleigh numbers based on gap width and boundary layer length in the range 165–2.0×10^9 and 2.9×10^6–3.0×10^{10}, respectively.

TEMPERATURE PROFILE RESULTS

The temperature profiles were obtained at two vertical sections: one section perpendicular to and through the center of the outer cube (referred to hereafter as the perpendicular plane) and the other section through the outer cube diagonal and through the center of the inner cube (hereafter referred to as the diagonal plane). The temperature profiles were plotted in terms of a dimensionless radius ratio and a dimensionless temperature ratio. For a given angular probe location, θ, the dimensionless radius ratio ranges from 0 at the inner body to 1 at the outer body. The dimensionless temperature ratio ranges from 1 to 0 between these same limits.

The characteristic length dimension used with the temperature profiles was G, the total outer body height minus the total inner body height divided by 2. Some flow visualization results are presented to supplement the temperature profiles (a detailed flow visualization study has been made and these results will be published separately).

Other investigators [13–18] have found that the form of the temperature profile for a given value of θ was independent of the temperature difference, ΔT, between the inner and outer bodies when the Prandtl number remained essentially constant. This was also true for the temperature profiles obtained with the cubical enclosure. The basic shape of the temperature profiles was invariant with changes in ΔT, and the magnitude of the mid-range dimensionless temperature generally increased with increasing ΔT. The absence of any

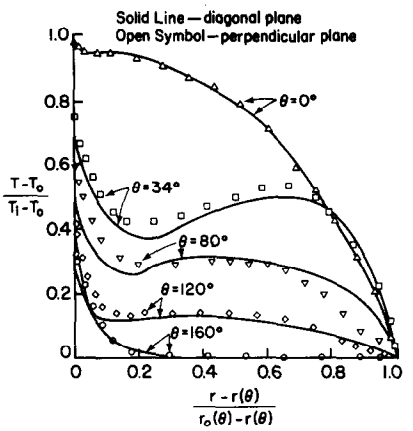

FIG. 11. Comparison of the perpendicular and diagonal planes, 17.78 × 20.5 cm cylinder ($G/r_i = 0.34$) and glycerin, $Pr = 4104$ and $\Delta T = 26.26$ K.

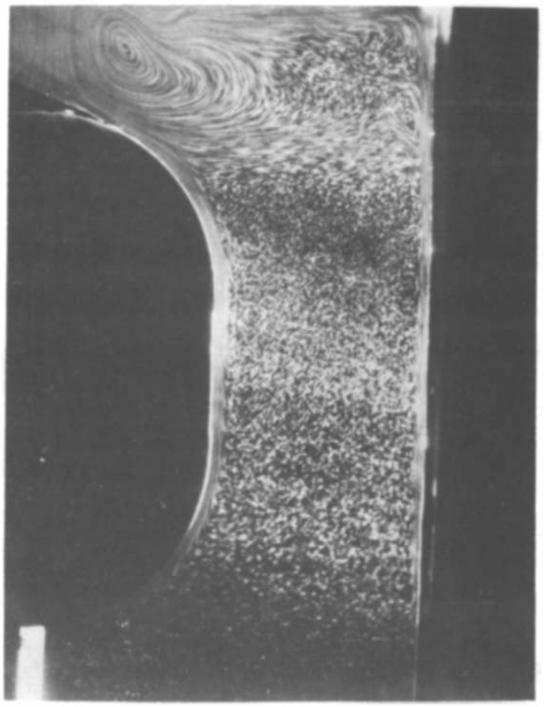

FIG. 12. Flow pattern for the 11.43 × 16.13 cm cylinder 20 CS fluid, $\Delta T = 9.05$ K.

influence of ΔT on the flow patterns was also observed for all fluids studied.

Evident in Fig. 11, and the profiles to follow, is that these temperature profiles can be described in terms of five distinct regions [13–18]. These regions are; steep gradient regions adjacent to the body surfaces, a region of small temperature gradients and inner and outer transition regions. The magnitude of the temperature drop adjacent to the inner body is generally greater than that at the outer surface due to the larger velocity in the boundary layer adjacent to the inner body. In the region of small temperature gradients the magnitude of the temperature, in general, decreases with increasing θ. This has been explained by previous investigators [14] and is due to the progressive heating of the fluid by the inner body as θ decreases and the cooling by the outer body as θ increases. At $\theta = 160°$ the convective activity is almost negligible, as was seen in the flow visualization results. In this region conduction, rather than convection, is the primary mechanism for the heat transfer. Another trend common to most of the temperature profiles is shown in Fig. 11 for the 17.73 × 20.57 cm cylinder and glycerin. There is practically no difference between the temperature profiles in the perpendicular and diagonal planes. As a consequence of this result, the diagonal plane will not be included with the temperature distributions.

The effect of the Prandtl number on the temperature profiles for the cubical enclosure was similar to that previously noted for the spherical enclosure [13–18]. Under the conditions for the form of the temperature profiles to be independent of ΔT, the tendency for mid-range dimensionless temperatures to increase with increasing Prandtl number was observed. This is particularly evident in the region of small temperature gradients. Comparing the liquids (20 CS and glycerin) it is seen that the effect of increasing the Prandtl number is to increase the radial extent of both the regions of steep gradients and the transition regions. This is primarily due to a thickening of the boundary layers. The profiles for air exhibit larger transition regions and more convective activity at $\theta = 160°$ than do the liquids. These results were confirmed by the flow visualization studies.

Temperature inversions can be seen in Fig. 11 (and in temperature profiles to be presented) for the 20 CS fluid and glycerin. These temperature inversions occurred primarily at $\theta = 34°$ and for a dimensionless radius ratio between 0.6 and 0.9. Liu *et al.* [5] first noted these temperature inversions and attributed them to the high rate of angular convection of heat relative to the radial transport of heat. This conclusion is supported by Fig. 12. The temperature inversions tended to increase in

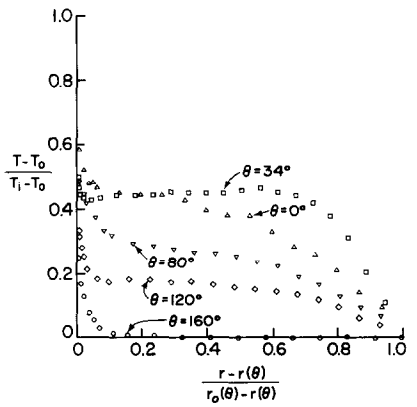

FIG. 13. Temperature profiles for the 22.86 cm sphere ($G/R = 0.17$) and 20 CS fluid; $\Delta T = 31.11$ K, $Pr = 231$ perpendicular plane.

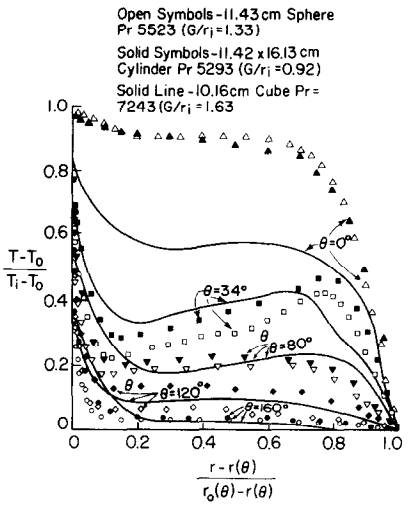

FIG. 14. Comparison of the temperature profiles for the different body types and glycerin, perpendicular plane.

FIG. 15. Flow patterns for the 11.43 × 22.61 cm cylinder and air, $\Delta T = 8.33$ K.

magnitude and in radial extent with increasing Prandtl number. Previous investigators [5, 14] have found that these inversions occur for $Ra_G \geqslant 5 \times 10^5$. In this study temperature profiles for air reached values of $Ra_G = 8 \times 10^5$ with no inversions evident. In addition, with the same inner body, a value of $Ra_G = 7 \times 10^5$ yielded no temperature inversions for the 20 CS fluid while a value of $Ra_G = 2 \times 10^5$ yielded significant temperature inversions with glycerin temperature profiles, for which Ra_G had a lower limit of 4×10^4. The Prandtl number does seem to have considerably more influence on the magnitude, extent and occurrence of these temperature inversions than can be included in the Rayleigh number alone.

The consistent ordering of the temperature profiles, seen above for the spherical and cylindrical inner bodies, was altered significantly as G/r_i decreased. This is shown in Fig. 13 for a spherical inner body with $G/r_i = 0.17$. It is clear that the magnitude of the temperature for $\theta = 0°$ is less than the value of the temperature for $\theta = 34°$ over most of the gap. The unusual ordering is caused by multicellular flow patterns seen in the flow visualization studies. The main cell in the lower portion of the gap extends into the upper gap region through $\theta = 34°$. The region in the vicinity of $\theta = 0°$ is multicellular and characterized by a somewhat random and 3-D flow. The flow pattern behavior described above occurred for all $G/r_i \leqslant 0.34$ for the cylindrical and spherical inner bodies and all the fluids.

The spherical, cylindrical and cubical inner body temperature profiles are presented on a common graph in Fig. 14. The conditions for the profiles to be independent of ΔT have been met in this figure. There is a striking similarity in the form of the temperature profiles for each of the inner body types. It might be expected that for a given θ, the dimensionless temperature would increase with a decrease in G/r_i. This was true for the profiles obtained with the spherical and cylindrical inner bodies. The magnitude of the mid-range temperature for the cubical inner bodies was generally greater than the corresponding temperature for the other inner body shapes. The larger surface area of the cube for a given r_i and increased convective activity due to unsteady, 3-D nature of the flow with the cubical inner body are two possible explanations.

The behavior of the profiles at $\theta = 0°$ in Fig. 14 (and in previous figures) is considerably different than the behavior at the other angular positions. This was also noted by Bishop *et al.* [13] and Scanlan *et al.* [14] for concentric spheres. They postulated a corner eddy near

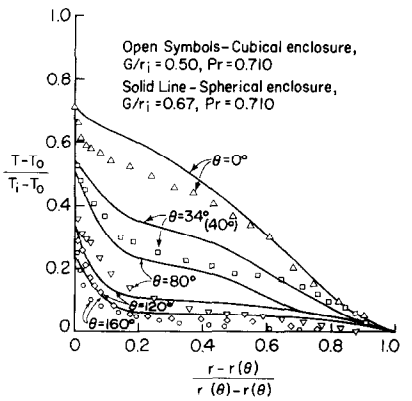

FIG. 16. Comparison of the temperature for the sphere–sphere [13] and sphere–cube geometries; air, perpendicular plane.

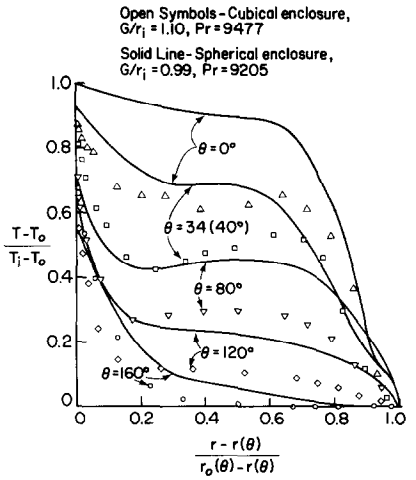

FIG. 17. Comparison of the temperature profiles for the cube–sphere and cube–cube geometries; glycerin, cube–sphere perpendicular plane [22].

the top of the inner spheres. The behavior at $\theta = 0°$ for the cylinder–sphere geometry was explained by McCoy *et al.* [17] as due to flow separation effects. These results were later confirmed with flow visualization data [18]. The flow separation and corner eddy are both present in Fig. 15 for the 11.43 × 22.61 cm cylindrical inner body and air.

A final comparison is made in Figs. 16 and 17 between the temperature profiles for the spherical and cubical enclosures with a common inner body type. All of the profiles satisfy the conditions for the form of the temperature profiles to be independent of ΔT. Evident from the figures is the minor effect the outer body shape has on the form of the temperature profiles. The magnitude of the mid-range dimensionless temperature at a given value of θ is generally greater for the spherical enclosure. This can be attributed to the larger surface area of the cubical outer body for a given value of r_o.

CONCLUSION

This study, through the use of three new geometries, has increased the amount of heat transfer and temperature profile data currently available on natural convection within enclosures. In addition, this study has made a fairly complete comparison of most of the data available for natural convection heat transfer between concentrically located 3-D isothermal inner bodies and 3-D isothermal outer bodies. Particular emphasis has been placed on the effects of different outer enclosures on the overall heat transfer with the variety of shapes employed in these experiments, local geometry effects must be evident, but emphasis is placed on more general geometric effects.

Comparisons made between the dimensionless temperature profiles for the different inner body types, and the cubical enclosure, displayed remarkable similarity. This was also true of comparisons made of the dimensionless temperature profiles for the spherical and cubical enclosures. In both these cases the form of the dimensionless temperature profiles was practically invariant with changes in inner and outer body geometries.

Comparisons made between the spherical and cubical enclosures, for the same inner body types, showed that the cubical enclosure resulted in a larger Nusselt number for a given Rayleigh number and inner body size. This difference always decreased as the size of the inner body decreased.

Non-isothermal inner body heat transfer data were also obtained in this study. It was found that the isothermality condition on the inner body could be relaxed, thereby increasing the usefulness of the heat transfer correlations.

Overall, the results have shown that the enclosure shape has only a small effect on the temperature profile and heat transfer results, while the enclosure dimensions have a significant effect on these results. The many different flow patterns and temperature profiles, whether unsteady or not, had very little effect on the overall heat transfer. The empirical equations given above should be used to predict the heat transfer by natural convection between a body and its enclosure whenever correlations for specific geometries and fluids are not available.

REFERENCES

1. G. K. Batchelor, Heat transfer by free convection across a closed cavity between vertical boundaries at different temperatures, *Q. J. Appl. Math.* **XII**, 209–233 (1954).
2. G. Poots, Heat transfer by laminar free convection in enclosed plane gas layers, *Q. J. Mech. Appl. Math.* **XI**(3), 257–273 (1958).
3. E. R. G. Eckert and W. O. Carlson, Natural convection in an air layer enclosed between vertical boundaries at different temperatures, *Int. J. Heat Mass Transfer* **2**, 106–120 (1961).
4. J. W. Elder, Laminar free convection in a vertical slot, *J. Fluid Mech.* **23**(1), 77–98 (1965).
5. C. Liu, W. K. Mueller and F. Landis, Natural convection heat transfer in long horizontal concentric annuli, paper 117 in *International Developments in Heat Transfer*, Part V, pp. 976–984 (1961).
6. J. Lis, Experimental investigation of natural convection heat transfer in simple and obstructed horizontal annuli, *Proc. 3rd Int. Heat Transfer Conf.*, Session 6, Vol. 2, pp. 196–204, New York (1966).
7. U. Grigull and W. Hauf, Natural convection in horizontal concentric annuli, *Proc. 3rd Int. Heat Transfer Conf.*, Session 6, Vol. 2, pp. 182–195, New York (1966).
8. E. H. Bishop, C. T. Carley and R. E. Powe, Natural convective oscillatory flow in cylindrical annuli, *Int. J. Heat Mass Transfer* **11**, 1741–1752 (1968).
9. R. E. Powe, C. T. Carley and E. H. Bishop, Free convective flow patterns in cylindrical annuli, *Trans. Am. Soc. Mech. Engrs*, Series C, *J. Heat Transfer* **88**, 310–314 (1969).
10. R. E. Powe, C. T. Carley and S. Carruth, A numerical solution for natural convection in cylindrical annuli, *Trans. Am. Soc. Mech. Engrs*, Series C, *J. Heat Transfer* **89**, 210–220 (1971).
11. M. R. Abbot, A numerical method for solving the equations of natural convection in a narrow concentric

cylindrical annulus with a horizontal axis, *Q. J. Mech. Appl. Math.* **XVII**(4), 471–481 (1964).
12. L. R. Mack and E. H. Bishop, Natural convection between horizontal concentric cylinders for low Rayleigh numbers, *Q. J. Mech. Appl. Math.* **XXI**(2), 223–241 (1968).
13. E. H. Bishop, L. R. Mack and J. A. Scanlan, Heat transfer by natural convection between concentric spheres, *Int. J. Heat Mass Transfer* **9**, 649–661 (1966).
14. J. A. Scanlan, E. H. Bishop and R. E. Powe, Natural convection between concentric spheres, *Int. J. Heat Mass Transfer* **13**, 1857–1872 (1970).
15. N. Weber, R. E. Powe, E. H. Bishop and J. A. Scanlan, Heat transfer by natural convection between vertically eccentric spheres, *Trans. Am. Soc. Mech. Engrs*, Series C, *J. Heat Transfer* **95**, 47–52 (1973).
16. S. H. Yin, R. E. Powe, J. A. Scanlan and E. H. Bishop, Natural convection flow patterns in spherical annuli, *Int. J. Heat Mass Transfer* **16**, 1785–1795 (1973).
17. C. T. McCoy, R. E. Powe, E. H. Bishop, N. Weber and J. A. Scanlan, Free convection between a vertical cylinder and a spherical enclosure, *Proc. 5th Int. Heat Transfer Conf.*, Tokyo (1974).
18. R. E. Powe, R. C. Baughman, J. A. Scanlan and J. T. Teng, Free convective flow patterns between a body and its spherical enclosure, *Trans. Am. Soc. Mech. Engrs*, Series C, *J. Heat Transfer* **97**, 296–298 (1975).
19. R. E. Powe, Bounding effects on the heat loss by free convection from spheres and cylinders, *Trans. Am. Soc. Mech. Engrs*, Series C, *J. Heat Transfer* **99**, 558–560 (1974).
20. L. R. Mack and H. C. Hardee, Natural convection between concentric spheres at low Rayleigh numbers, *Int. J. Heat Mass Transfer* **11**, 387–396 (1968).
21. R. E. Powe, R. O. Warrington and J. A. Scanlan, Natural convective flow between a body and its spherical enclosure, *Int. J. Heat Mass Transfer* **23**, 1337–1350 (1980).
22. R. E. Powe, R. O. Warrington and J. A. Scanlan, Natural convection heat transfer between bodies and their spherical enclosure, 19th National Heat Transfer Conf., Orlando, Florida (1980).
23. R. O. Warrington and G. Crupper, Natural convection heat transfer between cylindrical tube bundles and a cubical enclosure, *J. Heat Transfer* (in press).
24. T. Itoh, N. Fujita, N. Nishiwaki and M. Hirata, A new method of correlating heat transfer coefficients for natural convection in horizontal cylindrical annuli, *Int. J. Heat Mass Transfer* **13**, 1364–1368 (1970).
25. J. H. Lienhard, On the commonality of equations for natural convection from immersed bodies, *Int. J. Heat Mass Transfer* **16**, 2121–2123 (1973).
26. G. D. Raithby and K. G. T. Hollands, A general method of obtaining approximate solutions to laminar and turbulent free convection problems, *Advances in Heat Transfer*, Vol. II, pp. 265–315. Academic Press, New York (1975).
27. G. D. Raithby and K. G. T. Hollands, Analysis of heat transfer by natural convection (or film condensation for three dimensional flows), 6th Int. Heat Transfer Conf., Toronto (1978).

LE TRANSFERT THERMIQUE PAR CONVECTION NATURELLE ENTRE DES CORPS ET LEUR ENCEINTE

Résumé—On étudie expérimentalement la convection naturelle et le transfert thermique entre une enceinte cubique isotherme et des corps isothermes placés au centre, de forme sphérique, cylindrique et cubique. Des comparaisons sont faites avec les données existantes pour ces mêmes corps et une enceinte sphérique. De plus, des distributions de température et des données de visualisation sont obtenues pour la plupart des géométries. Des comparaisons sont faites entre les enceintes sphérique et cubique pour les mêmes types de corps internes, et elles montrent que l'enceinte cubique conduit à un nombre de Nusselt plus grand pour un nombre de Rayleigh et une dimension de corps interne donnés. Des données avec corps interne non isotherme montrent que les conditions de non isothermicité peuvent être relaxées. Tous les résultats de transfert thermique sont rassemblés avec une déviation moyenne inférieure à 14%. Globalement l'effet de la forme de l'enceinte est faible lorsqu'on emploie une échelle de longueur appropriée.

WÄRMEÜBERTRAGUNG DURCH NATÜRLICHE KONVEKTION ZWISCHEN KÖRPERN UND HOHLRÄUMEN

Zusammenfassung—Die Wärmeübertragung durch natürliche Konvektion zwischen einem isothermen inneren Körper (Kugel, Zylinder, Würfel) und einem dazu konzentrisch angeordneten isothermen äußeren Körper (Würfel) wurde experimentell untersucht. Die Ergebnisse wurden mit bekannten Daten für dieselben inneren Körper in einem kugelförmigen Hohlraum verglichen. Zusätzlich wurden für die meisten dieser Anordnungen die Temperaturverteilung bestimmt und die Strömung sichtbar gemacht. Der Vergleich zwischen kugel- und würfelförmigem Hohlraum (bei gleichen Einbauten) zeigte, daß sich bei der Würfelform für eine bestimmte Rayleigh-Zahl und Größe des inneren Körpers größere Nusselt-Zahlen ergaben. Sämtliche Wärmeübergangsdaten wurden bei einer mittleren Abweichung von weniger als 14% korreliert. Insgesamt war der Einfluß der Form des Hohlraums klein, solange eine geeignete Bezugslänge verwendet wurde.

ТЕПЛООБМЕН ЕСТЕСТВЕННОЙ КОНВЕКЦИЕЙ МЕЖДУ ТЕЛАМИ И СРЕДОЙ, В КОТОРУЮ ОНИ ПОМЕЩЕНЫ

Аннотация—Экспериментально изучен естественноконвективный теплообмен между концентрично расположенными изотермическими сферическими, цилиндрическими и кубическими телами и изотермическими кубическими полостями, в которых они расположены. Проведено сравнение с имеющимися результатами для этих же тел и сферической полости. Для большинства этих геометрий также получены распределения температур и данные по визуализации течения. Сравнения, проведенные между сферической и кубической полостями для вышеуказанных геометрий тел показали, что в кубической полости для заданных чисел Рэлея и размера внутреннего тела число Нуссельта больше. Данные по теплообмену для неизотермического внутреннего тела свидетельствуют о том, что условия неизотермичности на теле могут быть ослаблены. Все результаты по теплообмену обобщены со средним отклонением, не превышающим 14%. Установлено, что влияние формы полости мало, если выбрать соответствующий линейный масштаб.